J Solid State Electrochem (2017) 21:2349–2354
DOI 10.1007/s10008-017-3588-1

ORIGINAL PAPER

Electrodeposition of polyaniline in long TiO_2 nanotube arrays for high-areal capacitance supercapacitor electrodes

Ji Xing[1,2] · Weikang Zhang[1] · Min Yin[2] · Xufei Zhu[1] · Dongdong Li[2] · Ye Song[1]

Received: 4 January 2017 / Revised: 12 March 2017 / Accepted: 31 March 2017 / Published online: 7 April 2017

Abstract Anodic TiO_2 nanotube arrays (TNTAs) were found to be a suitable scaffold for the loading of other active materials for supercapacitors. The prepared coaxial nanostructured composite-based TNTAs have been reported to show a remarkable specific capacitance. However, owing to the semiconductive nature of TiO_2 and the diffusion limits of electrolytes in nanotubes, the electrodeposition of active materials was often found to preferentially occur at the upper areas of TNTAs, resulting in insufficient pore filling especially for long nanotubes. Here, robust and long (over 100 μm) TNTAs are served as a support template for electrodeposition of polyaniline (PANI). After an electrochemical reduction process of TNTAs, uniform and complete pore filling with PANI using electrodeposition from bottom to top is realized by potentiodynamic cycling successfully. The obtained PANI/TNTAs composites show areal capacitances as high as 512.4 mF cm^{-2} due to the higher loadings of PANI. They also have relatively good rate capability and cycling stability. This work makes PANI/TNTAs composite electrodes really scalable.

Keywords Long TiO_2 nanotubes · Electrodeposition · Polyaniline · Supercapacitor · High areal capacitance

✉ Dongdong Li
lidd@sari.ac.cn

✉ Ye Song
soong_ye@sohu.com

[1] Key Laboratory of Soft Chemistry and Functional Materials of Education Ministry, Nanjing University of Science and Technology, Nanjing 210094, People's Republic of China

[2] Shanghai Advanced Research Institute, Chinese Academy of Sciences, 99 Haike Road, Zhangjiang Hi-Tech Park, Pudong, Shanghai 201210, People's Republic of China

Introduction

Anodic TiO_2 nanotube arrays (TNTAs) grown in situ on Ti substrates, which can be utilized directly as an electrode without the need for any binder, have found widespread applications in photovoltaic cells [1–5], photoelectrochemical water splitting [6, 7], and supercapacitors [8, 9]. For application as an electrode for supercapacitors, achieving higher capacitance is always a key research target. Unfortunately, TNTAs show a low specific capacitance (~10 mF cm^{-2} at best to date), which is not yet competitive with typical materials for supercapacitors such as RuO_2 [10, 11]. To enhance their specific capacitance, one of the most straightforward and common way is the manufacture of composites with other active materials for supercapacitors because TNTAs were found to be a suitable scaffold for the loading of these materials. The prepared coaxial nanostructured composite-based TNTAs have been reported to show a remarkable specific capacitance [12–16]. However, it is not easy to attain the complete filling of nanotubes with active materials. At present, electrodeposition is a frequently used method to fill the active materials into nanotubes. Nonetheless, the active materials were often found to reside dominantly at the upper areas of TNTAs, resulting in insufficient pore filling, although there is electrically driving force in this case (under the action of an applied electric field). For instance, the electrodeposition of polyaniline (PANI) onto TNTAs has been investigated heavily, but the SEM images provided by many researchers demonstrated that PANI nanowires were only deposited on the surface of TNTAs instead of inside nanotubes [15–19]. Due to the semiconductive nature of TiO_2 and the diffusion limits of electrolytes in nanotubes, the electrodeposition of PANI occurs more easily on the surface of TNTAs than in nanotubes. Similar behavior can also be observed in the electrodeposition of MnO_2 [12, 13] or WO_3 [20] onto TNTAs. Furthermore, it should be noted that the

TNTAs with short nanotubes (usually a few micrometers) was utilized in those electrodeposition experiments reported previously [12, 15, 16, 19, 21]. For the TNTAs with long nanotubes, realization of sufficient pore filling would become more difficult because of the longer diffusional path of electrolytes along the nanotubes.

Most recently, we have successfully fabricated long TNTAs (over 100 μm) with satisfactory mechanical adhesion to Ti substrate [9]. The long TNTAs with a much higher surface area of tubular structures can allow larger loading capacity of active materials, resulting in a significant improvement in specific capacitance. In this work, an effective approach was developed to solve the abovementioned problem. As an example, PANI was successfully electrodeposited into the long TNTAs by potentiodynamic cycling. As expected, the obtained PANI/TNTA composite electrodes yielded a drastically enhanced areal capacitance.

Experimental

TNTAs with a thickness of ~100 μm were fabricated by galvanostatic anodization of Ti foils (99.9% purity, 0.5-mm thickness) in an ethylene glycol (EG) electrolyte containing 0.3 wt% NH_4F and 2 vol% deionized water at a current density of 10 mA cm^{-2} for 4 h at room temperature (~24 °C). Then, the prepared TNTAs were anodized again in 5 wt% H_3PO_4 in EG electrolyte to reinforce the adhesion of nanotubes to Ti substrate [22] and crystallized by annealing at 450 °C in argon atmosphere for 3 h. Here, this second anodization treatment is similar to the bottom sealing procedures reported by Lee et al. [23]. After this step, it was found that the long TNTAs become robust and more adherent to Ti substrate and can withstand the subsequent annealing. A detailed description of preparation and treatment of long TNTAs can be found elsewhere [9].

Before electrodeposition of PANI, long TNTA films with active area of 0.5 cm^2 were electrochemically reduced by cyclic voltammetry (CV) in 1 M NH_4Cl aqueous solution from −1.2 to −0.2 V at a scan rate of 100 mV s^{-1} for 10 cycles [24]. This electrochemical reduction process can make the bottom layer of TNTAs more conductive than their walls so that PANI is expected to be electrodeposited starting from the bottom [24]. The electropolymerization of aniline was performed in a solution containing 0.1 M aniline and 0.5 M H_2SO_4, either potentiostatically (at 0.7 V) or by CV (from −0.2 to 1.0 V at a scan rate of 25 mV s^{-1}). Prior to the capacitive performance tests, an electrochemical hydrogenation doping of the as-prepared PANI/TNTAs composite films was performed in 0.5 M Na_2SO_4 solution at −1.5 V for 60 s to further enhance the conductivity of TNTAs [25, 26]. The whole process is illustrated in Fig. 1. All the electrochemical experiments were carried out in a three-electrode configuration with a saturated calomel electrode (SCE) as reference electrode and a carbon rod as counter electrode.

The morphology of samples was examined by field-emission scanning electron microscope (SEM, FEI Quanta 250FEG). The crystal structure of the TiO_2 samples was examined by X-ray diffractometer (XRD, Bruker-AXS D8 ADVANCE at 40-kV voltage and 40-mA current with Cu-Kα radiation). Mott-Schottky plots were measured at 10 kHz in 0.5 M Na_2SO_4 solution. Supercapacitive performances of the samples were evaluated in 0.5 M H_2SO_4 solution using AUTOLAB PGSTAT302 N/FRA2. CV tests were performed between −0.3 and 0.6 V at different scan rates over the range from 10 to 200 mV s^{-1}, and galvanostatic charge-discharge tests were carried out over the same potential range at different current densities from 0.5 to 10 mA cm^{-2}.

Results and discussion

Figure 2 shows SEM images of the prepared long TNTAs obtained for 4-h galvanostatic anodization at 10 mA cm^{-2}. It can be found that the inner diameter of the nanotubes decreases gradually from top to bottom by comparing Fig. 2a–c. In fluoride-containing electrolytes, the nanotube wall thickness is inevitably affected by chemical etching during anodization. As the etching is exposure time dependent, the inner diameter of the nanotubes decreases gradually from top to bottom, exhibiting a V-shaped sidewall thickness profile [27]. As shown in Fig. 2d, TNTAs with a thickness of over 100 μm can be obtained after 4-h anodization at 10 mA cm^{-2}. It should be mentioned that anodization at 10 mA cm^{-2} not only has higher growth rate of TNTAs but also does not lead to cracks or collapse of nanotube layer [9]. This is the reason why this current density was applied here for fabricating TNTAs using a constant current anodization technique.

As mentioned above, uniform pore filling with PANI by electrodeposition from the tube bottom to the top is hard to achieve. To solve this problem, a reductive doping process for TNTAs was carried out to form a high-conductivity bottom

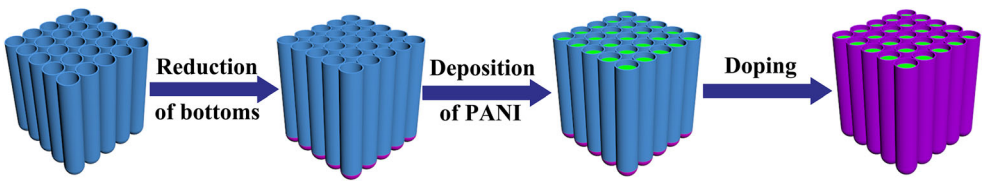

Fig. 1 Schematic diagram of fabrication protocol for the PANI/TNTA composite films

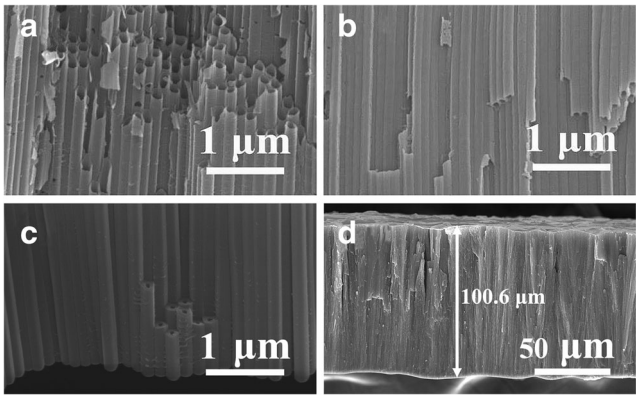

Fig. 2 SEM images of long TNTAs taken **a** at the top, **b** in the middle, and **c** close to the bottom of nanotubes. **d** Cross-sectional view showing a whole image of the TNTA layer

layer of nanotubes before electrodeposition (Fig. 1). Thus, the electrochemical polymerization of aniline should occur starting from the bottom of nanotubes. In this study, the electrodeposition of PANI in long TNTAs was tried by both potentiostatic and potentiodynamic cycling techniques. Figure 3a shows a typical chronoamperogram during the potentiostatical deposition of PANI at 0.7 V for 600 s. It is seen that the current rapidly decays to a minimum after an initial current pulse, which corresponds to a period of induction where the double-layer charge and the monomer oxidation occur [28]. The current begins to increase obviously after 300 s, indicating an increased electrodeposition rate owing to the self-catalyzing effect of PANI [29, 30]. After potentiostatical deposition of 600 s, a layer of black products on the surface of TNTA films was observed with the naked eye, demonstrating the formation of PANI on the film surface. However, SEM observations reveal that no electrodeposition product can be found inside the nanotubes although the surface of TNTAs is covered by PANI films as shown in Fig. 3c, d, showing that an attempt to fill nanotubes with PANI by the potentiostatical electrodeposition failed.

Fortunately, a uniform growth of PANI in nanotubes from bottom to top can be realized by CV at a scan rate of 25 mV s^{-1}. While using CV technique, no product on the surface of TNTAs was observed with the naked eye after 15 potentiodynamic cycles, but the cyclic voltammograms recorded during electropolymerization showed typical redox peaks of PANI (Fig. 3b), implying the existence of PANI inside the nanotubes. Unlike the electropolymerization of aniline on flat substrates [31], it is seen from Fig. 3b that the increment of redox peak currents during each cycle tends to decrease gradually with cycle number and the oxidation (reduction) peak slightly shifts toward a more positive (negative) potential. The result implies that the electropolymerization of aniline into TNTAs becomes more

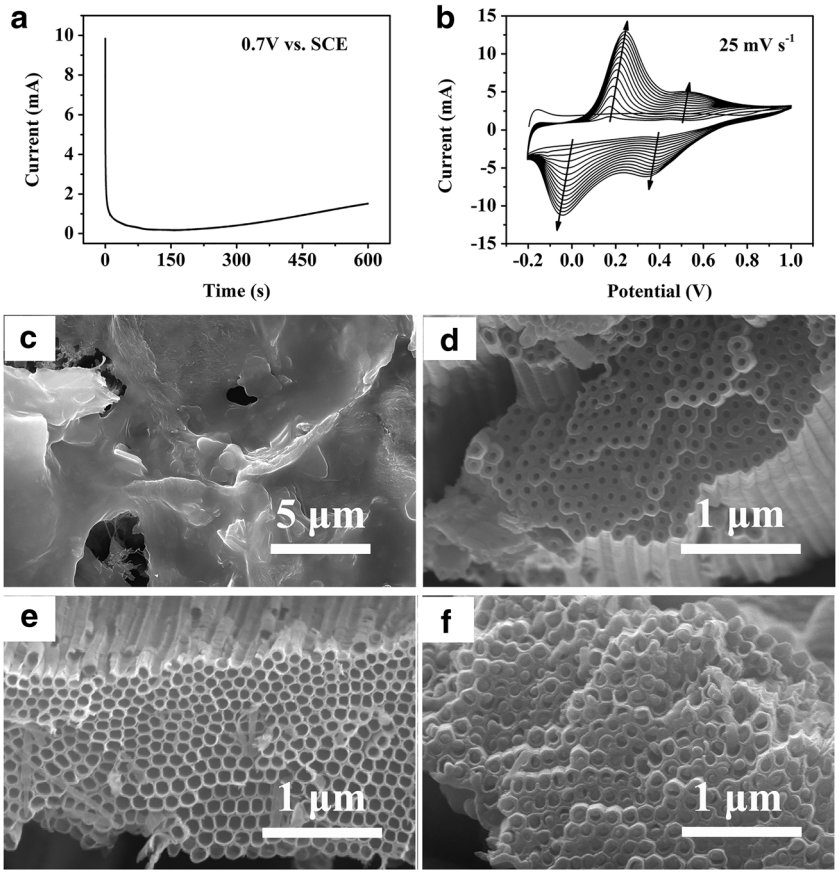

Fig. 3 Curves of electrochemical polymerization of aniline by **a** potentiostatic (0.7 V) and **b** CV methods. SEM images of the as-prepared PANI/TNTA composite structures by potentiostatic method, **c** top surface and **d** near the bottom, and by CV method, **e** top surface and **f** near the middle part of nanotubes

and more difficult as the cycle number increases, possibly because the diffusion rate of aniline monomer into nanotubes is lower than the scan rate. For the potentiodynamic electrodeposition, the electropolymerization of aniline occurs only at a high anodic potential, whereas the electropolymerization proceeds continuously for the potentiostatic method. Thus, there is a break in deposition in between two consecutive potential sweeps, which is beneficial to diffusion of monomer into nanotubes. Besides, unlike the potentiostatic case, the formed PANI can be in the highly conducting state during potentiodynamic cycling; this facilitates the subsequent electrodeposition of PANI on the formed PANI within nanotubes. Consequently, the complete filling of nanotubes with PANI is available. Figure 3e, f shows the morphology of the tube tops of TNTAs and the TNTAs taken from the fractures in the middle of nanotubes after electrodeposition of PANI, respectively. As can be seen, almost all nanotubes near the middle part of the TNTA layer are filled with PANI completely, indicating that PANI/TNTA composite structures can be achieved by potentiodynamic cycling (Fig. 3f). In contrast, there is nothing in nanotubes near their surface as shown in Fig. 3e, confirming the above-observed result by the naked eye, i.e., no electrodeposition product on the surface of TNTAs. This indicates that PANI does not grow out of the nanotubes after 15 potentiodynamic cycles. In fact, too much potentiodynamic cycles may lead to the formation of PANI on the nanotube surface; thus, one cannot distinguish whether the electrodeposition of PANI occurs within nanotubes or on their surface. To avoid this problem, the electrodeposition of PANI was carried out by CV only after 15 cycles in this work. In conclusion, the above SEM images demonstrate that PANI grows in nanotubes indeed from bottom to top.

Figure 4a shows the evolution of the XRD patterns of TNTAs during the whole process illustrated in Fig. 1 for the fabrication of the PANI/TNTA composite structures. Clearly, the as-anodized TNTAs are amorphous because no diffraction peak can be observed except for the peaks originated from Ti substrates, in agreement with previous works [32, 33]. It is seen that the TNTAs were transformed from amorphous to anatase phase with the strongest (004) diffraction peak after annealing in argon. Moreover, all of the XRD patterns show no noticeable distinction during the subsequent treatment procedures, including the electrochemical reduction of nanotube bottoms, the electrodeposition of PANI, and the electrochemical hydrogenation doping. The results suggest that these treatments have no effect on the crystal structure of TNTAs, in accordance with previous studies [9, 26, 34]. Especially, due to the amorphous nature of PANI, the TNTA/PANI samples have similar XRD pattern as TNTAs. In addition, the TNTA/PANI samples were found to have no noticeable change in the morphology and crystal structure after the electrochemical hydrogenation doping [24]. Nevertheless, it has been demonstrated that this treatment step can significantly enhance the conductivity of TNTAs due to the increased oxygen vacancies (or Ti^{3+}) and the introduction of the interstitial ionized hydrogen [9, 26]. Furthermore, the increase in carrier density of TNTAs after the electrochemical doping can be also confirmed by Mott-Schottky analysis. Figure 4b shows Mott-Schottky plots of the TNTA samples before and after the electrochemical doping, which were obtained from capacitances derived from the electrochemical impedance data at each potential. Based on Mott-Schottky equation [12, 35], the carrier density of the samples after the electrochemical doping was calculated to increase from 1.1×10^{23} to 3.0×10^{23} cm^{-3}.

Cyclic voltammograms and the corresponding areal capacitance at various scan rates for the as-prepared PANI/TNTA composites are shown in Fig. 5a, b, respectively. The shape of the voltammograms remains relatively unchanged, and the areal capacitance decreases slowly as the scan rate increases, suggesting a high rate capability. The PANI/TNTA composites exhibit a pair of distinct redox peaks originated from PANI, leading to a larger pseudocapacitance. Therefore, the composites achieve a greatly increased areal capacitance of 512.4 mF cm^{-2} at 100 mV s^{-1} (Fig. 5b). Owing to the utilization of long TNTAs, this areal capacitance is 5.5 times larger than that of previously reported PANI/TNTA composites made from shorter nanotubes [36], confirming a higher loading of PANI in the TNTAs. Also, this areal capacitance is 4.5 times higher than that of bare TNTAs themselves because of the addition of PANI [9]. The as-prepared PANI/TNTAs

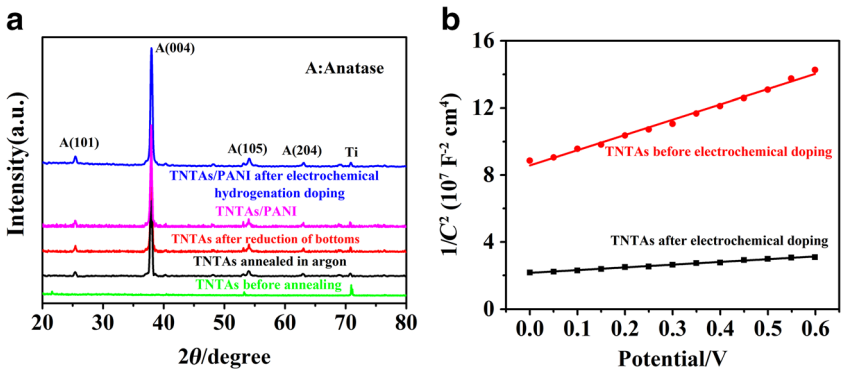

Fig. 4 **a** Evolution of the XRD patterns of TNTAs during the whole process illustrated in Fig. 1. **b** Mott-Schottky plots of the argon-annealed TNTAs before and after the electrochemical doping

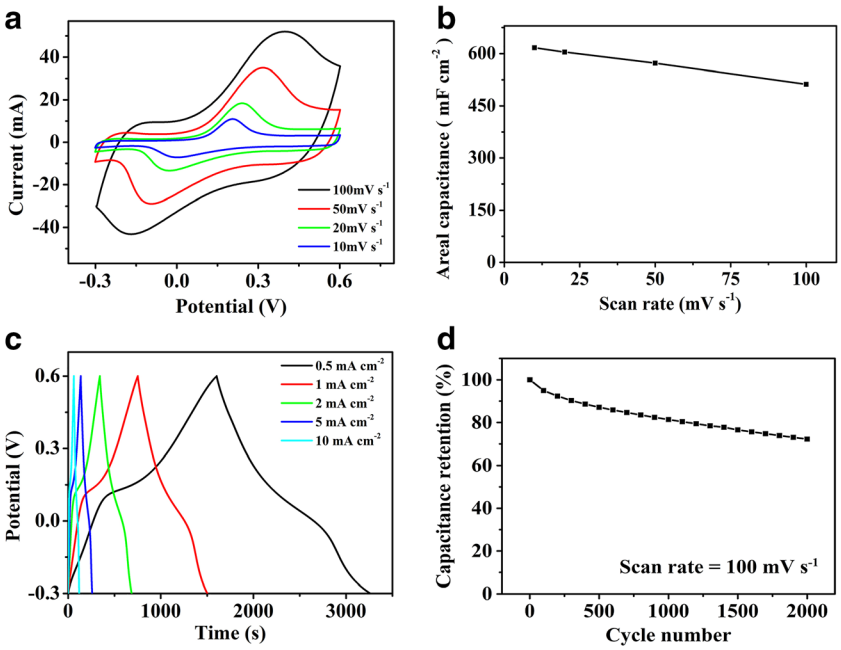

Fig. 5 **a** Cyclic voltammograms and **b** areal capacitance of the PANI/TNTAs at different scan rates (10~100 mV s^{-1}). **c** Galvanostatic charge-discharge curves of the PANI/TNTAs at different current densities (0.5~10 mA cm^{-2}). **d** Capacitance retention vs. cycle number up to 2000 cycles measured by CV test at 100 mV s^{-1}

composites can be steadily operated over a wide range of current densities from 0.5 to 10 mA cm^{-2} (Fig. 5c), which exhibits only 30.9% loss in capacitance with a 20 times increase in the discharge current density, also implying excellent rate capability. In addition, the nearly symmetrical charge-discharge curves at various current densities demonstrate good coulombic efficiency. As seen in Fig. 5d, the as-prepared PANI/TNTAs can remain 72.2% of the initial capacitance after 2000 cycles, suggesting a relatively good long-term cycling stability.

Conclusions

In summary, over 100-μm-thick TNTAs were served as suitable support templates for electrodeposition of PANI via electrochemical polymerization of aniline. After the electrochemical reduction process of TNTAs, uniform and complete pore filling with PANI by electrodeposition from bottom to top was achieved using potentiodynamic cycling. The prepared PANI/TNTA composites exhibit an areal capacitance of 512.4 mF cm^{-2}, well above that of the PANI/TNTA systems based on usually short TNTAs due to the higher loadings of PANI. Also, they have relatively good rate capability and cycling stability. Besides, the areal capacitance of the PANI/TNTAs is expected to improve further by tuning aniline concentration in polymerization solutions and potential sweep rates.

Acknowledgements This work was financially supported by the National Natural Science Foundation of China (Grant Nos. 51377085, 51577093, 61474128, and 61504155); Science and Technology Commission of Shanghai Municipality (14JC1492900); the Youth Innovation Promotion Association, Chinese Academy of Sciences (2013302); and the Youth Innovation Fund for Interdisciplinary Research of SARI (Y426475234).

References

1. Xu J, Wu H, Lu L, Leung SF, Chen D, Chen X, Fan Z, Shen G, Li D (2014) Integrated photo-supercapacitor based on bi-polar TiO_2 nanotube arrays with selective one-side plasma-assisted hydrogenation. Adv Funct Mater 24(13):1840–1846
2. Chong C, Li F, Li G, Tan F, Li S, Ling L (2014) Double-sided transparent electrodes of TiO_2 nanotube arrays for highly efficient CdS quantum dot-sensitized photoelectrodes. J Mater Sci 49(4): 1868–1874
3. Li D, Chien CJ, Deora S, Chang PC, Moulin E, Lu JG (2011) Prototype of a scalable core–shell Cu_2O/TiO_2 solar cell. Chem Phys Lett 501(4–6):446–450
4. Lee D, Kim HB, Yu S, Kim HJ, Lee WI, Jang DJ (2014) Facile fabrication of anatase TiO_2 nanotube arrays having high photocatalytic and photovoltaic performances by anodization of titanium in mixed viscous solvents. J Mater Sci 49(9):3414–3422
5. Li Z, Yu L, Liu Y, Sun S (2014) Enhanced photovoltaic performance of solar cell based on front-side illuminated CdSe/CdS double-sensitized TiO_2 nanotube arrays electrode. J Mater Sci 49(18):6392–6403
6. Xu Z, Lin Y, Yin M, Zhang H, Cheng C, Lu L, Xue X, Fan HJ, Chen X, Li D (2015) Understanding the enhancement mechanisms of surface plasmon-mediated photoelectrochemical electrodes: a case study on Au nanoparticle decorated TiO_2 nanotubes. Adv Mater Interfaces 2(13):1500169
7. Gui Q, Zhen X, Zhang H, Cheng C, Zhu X, Min Y, Ye S, Lu L, Chen X, Li D (2014) Enhanced photoelectrochemical water splitting performance of anodic TiO_2 nanotube arrays by surface passivation. ACS Appl Mater Interfaces 6(19):17053–17058
8. Zheng L, Dong Y, Bian H, Lee C, Lu J, Li YY (2016) Self-ordered nanotubular TiO_2 multilayers for high-performance photocatalysts and supercapacitors. Electrochim Acta 203:257–264

9. Zhang H, Chen Z, Song Y, Yin M, Li D, Zhu X, Chen X, Chang PC, Lu L (2016) Fabrication and supercapacitive performance of long anodic TiO_2 nanotube arrays using constant current anodization. Electrochem Commun 68:23–27
10. Burke A (2000) Ultracapacitors: why, how, and where is the technology. J Power Sources 91(1):37–50
11. Li X, Gan W, Zheng F, Li L, Zhu N, Huang X (2012) Preparation and electrochemical properties of RuO2/polyaniline electrodes for supercapacitors. Synth Met 162(11–12):953–957
12. Lu X, Wang G, Zhai T, Yu M, Gan J, Tong Y, Li Y (2012) Hydrogenated TiO_2 nanotube arrays for supercapacitors. Nano Lett 12(3):1690–1696
13. Dong S, Chen X, Gu L, Zhou X, Li L, Liu Z, Han P, Xu H, Yao J, Wang H, Zhang X, Shang C, Cui G, Chen L (2011) One dimensional MnO_2/titanium nitride nanotube coaxial arrays for high performance electrochemical capacitive energy storage. Energy Environ Sci 4(9):3502
14. Shang C, Dong S, Wang S, Xiao D, Han P, Wang X, Gu L, Cui G (2013) Coaxial $Ni_xCo_{2x}(OH)_{6x}$/TiN nanotube arrays as supercapacitor electrodes. ACS Nano 7(6):5430–5436
15. Xie K, Li J, Lai Y, Zhang Z, Liu Y, Zhang G, Huang H (2011) Polyaniline nanowire array encapsulated in titania nanotubes as a superior electrode for supercapacitors. Nano 3(5):2202–2207
16. Chen J, Xia Z, Li H, Li Q, Zhang Y (2015) Preparation of highly capacitive polyaniline/black TiO_2 nanotubes as supercapacitor electrode by hydrogenation and electrochemical deposition. Electrochim Acta 166:174–182
17. Huang H, Gan M, Ma L, Yu L, Hu H, Yang F, Li Y, Ge C (2015) Fabrication of polyaniline/graphene/titania nanotube arrays nanocomposite and their application in supercapacitors. J Alloys Compd 630:214–221
18. Palmas S, Mascia M, Vacca A, Llanos J, Mena E (2014) Analysis of photocurrent and capacitance of TiO_2 nanotube–polyaniline hybrid composites synthesized through electroreduction of an aryldiazonium salt. RSC Adv 4(46):23957
19. Shao Z, Li H, Li M, Li C, Qu C, Yang B (2015) Fabrication of polyaniline nanowire/ TiO_2 nanotube array electrode for supercapacitors. Energy 87:578–585
20. Reyes-Gil KR, Robinson DB (2013) WO3-enhanced TiO_2 nanotube photoanodes for solar water splitting with simultaneous wastewater treatment. ACS Appl Mater Interfaces 5(23):12400–12410
21. Tsui LK, Zangari G (2013) The influence of morphology of electrodeposited Cu2O and Fe_2O_3 on the conversion efficiency of TiO_2 nanotube photoelectrochemical solar cells. Electrochim Acta 100: 220–225
22. Yu D, Zhu X, Xu Z, Zhong X, Gui Q, Song Y, Zhang S, Chen X, Li D (2014) Facile method to enhance the adhesion of TiO_2 nanotube arrays to Ti substrate. ACS Appl Mater Interfaces 6(11):8001–8005
23. Lee K, Schmuki P (2013) Bottom sealing and photoelectrochemical properties of different types of anodic TiO_2 nanotubes. Electrochim Acta 100:229–235
24. Song Y, Lv H, Yang C, Xiao H, Chen X, Zhu X, Li D (2014) Enhanced electroactivity at physiological ph for polyaniline in three-dimensional titanium oxide nanotube matrix. Phys Chem Chem Phys 16(30):15796–15799
25. Li Z, Ding Y, Kang W, Li C, Lin D, Wang X, Chen Z, Wu M, Pan D (2015) Reduction mechanism and capacitive properties of highly electrochemically reduced TiO_2 nanotube arrays. Electrochim Acta 161:40–47
26. Wu H, Li D, Zhu X, Yang C, Liu D, Chen X, Song Y, Lu L (2014) High-performance and renewable supercapacitors based on TiO_2 nanotube array electrodes treated by an electrochemical doping approach. Electrochim Acta 116:129–136
27. Albu SP, Ghicov A, Aldabergenova S, Drechsel P, Leclere D, Thompson GE, Macak JM, Schmuki P (2008) Formation of double-walled TiO_2 nanotubes and robust anatase membranes. Adv Mater 20(21):4135–4139
28. Córdova R, Valle MAD, Arratia A, Gómez H, Schrebler R (1994) Effect of anions on the nucleation and growth mechanism of polyaniline. J Electroanal Chem 377(1–2):75–83
29. Genies EM, Tsintavis C (1985) Redox mechanism and electrochemical behaviour or polyaniline deposits. J Electroanal Chem 195(1):109–128
30. Du XF, Xu YL, Xiong LL, Bai Y, Zhu JB, Mao SC (2014) Polyaniline with high crystallinity degree: synthesis, structure, and electrochemical properties. J Appl Polym Sci 131(19):40827
31. Chen Z, Lv H, Zhu X, Li D, Zhang S, Chen X, Song Y (2014) Electropolymerization of aniline onto anodic WO_3 film: an approach to extend polyaniline electroactivity beyond pH 7. J Phys Chem C 118(47):27449–27458
32. Lee K, Mazare A, Schmuki P (2014) One-dimensional titanium dioxide nanomaterials: Nanotubes. Chem Rev 114(19):9385–9454
33. Liu N, Albu SP, Lee K, So S, Schmuki P (2012) Water annealing and other low temperature treatments of anodic TiO_2 nanotubes: a comparison of properties and efficiencies in dye sensitized solar cells and for water splitting. Electrochim Acta 82(21):98–102
34. Liu N, Schneider C, Freitag D, Hartmann M, Venkatesan U, Müller J, Spiecker E, Schmuki P (2014) Black TiO_2 nanotubes: cocatalyst-free open-circuit hydrogen generation. Nano Lett 14(6):3309–3313
35. Kontos AI, Likodimos V, Stergiopoulos T, Tsoukleris DS, Falaras P, Rabias I, Papavassiliou G, Kim D, Kunze J, Schmuki P (2010) Self-organized anodic TiO_2 nanotube arrays functionalized by iron oxide nanoparticles. Chem Mater 21(4):662–672
36. Xie S, Gan M, Ma L, Li Z, Yan J, Yin H, Shen X, Xu F, Zheng J, Zhang J, Hu J (2014) Synthesis of polyaniline-titania nanotube arrays hybrid composite via self-assembling and graft polymerization for supercapacitor application. Electrochim Acta 120(7):408–415